PLANT SCIENCES

A conserved module in the formation of moss midribs and seed plant axillary meristems

Yanhua Ge[1,2]†, Yi Gao[1]†, Yuling Jiao[2,3]*, Ying Wang[1]*

Different evolutionary lineages have evolved distinct characteristic body plans and anatomical structures, but their origins are largely elusive. For example, seed plants evolve axillary meristems to enable lateral branching. In moss, the phyllid (leaf) midrib containing specialized cells is responsible for water conduction and support. Midribs function like vascular tissues in flowering plants but may have risen from a different evolutionary path. Here, we demonstrate that midrib formation in the model moss *Physcomitrium patens* is regulated by orthologs of *Arabidopsis LATERAL SUPPRESSOR* (*LAS*), a key regulator of axillary meristem initiation. Midribs are missing in loss-of-function mutants, and ectopic formation of midrib-like structures is induced in overexpression lines. Furthermore, the *PpLAS*/*AtLAS* genes have conserved functions in the promotion of cell division in both lineages, which alleviates phenotypes in both *Physcomitrium* and *Arabidopsis las* mutants. Our results show that a conserved regulatory module is reused in divergent developmental programs, water-conducting and supporting tissues in moss, and axillary meristem initiation in seed plants.

INTRODUCTION

During evolution, new innovations in body plans and anatomy arise to allow adaptation to new growth habitats, which has occurred repetitively in different land plant lineages. The manner by which these new innovations are achieved is an outstanding question in biology, and the underlying molecular mechanisms remain largely unexplored. The axillary meristem (AM) is an innovation of seed plants; the generation of AMs associated with each leaf allows the formation of lateral branches that efficiently occupy space. Recent molecular genetic studies have identified several regulators of AM initiation, including LATERAL SUPPRESSOR in *Arabidopsis* (AtLAS hereafter), and its orthologs tomato Lateral Suppressor and rice MONOCULM1 (*1*–*3*). AtLAS is a putative transcription factor that belongs to the plant-specific GAI-RGA-and-SCR (GRAS) family. Previous studies have illustrated that loss-of-function mutations in *AtLAS* and its orthologs result in compromised boundary formation and defective AM formation (*1*). Since AMs are a seed plant–specific structure, the manner by which AM regulators, including AtLAS, have emerged and been recruited to control AM formation during evolution remains largely elusive. GRAS family genes are found in subaerial Zygnematophyceae (*4*), implicating an ancient origin and potential roles of *LAS* genes in terrestrial adaptation during plant evolution.

During the transition from aquatic to terrestrial habitats, internal systems that transport water and provide structural support are innovated in land plants to adapt to the environment. In vascular plants, the water-conducting activity is performed by tracheids and vessel elements in xylem. By contrast, some species of nonvascular mosses, as one of the earliest land plants, have evolved midribs in phyllids (hereafter called leaves) for water conduction and support (*5*, *6*). Despite the similarity in function, midribs are drastically different from, and much less branched than, the vasculature (*5*, *7*, *8*); therefore, the water transport efficiency of midribs is low and moss mainly relies on capillarity to externally transport water (*6*, *8*). In *Physcomitrium patens* (formerly known as *Physcomitrella patens*), midribs contain hydroid and stereid cells. Hydroids are thin-walled cells that are initially live, then undergo programmed cell death, and have a totally degenerated protoplasm upon maturation (*5*–*8*). By contrast, stereids have thickened cell walls and mainly serve the purpose of support (*8*). Although arguably different in origin (*8*), development of the moss midrib and flowering plant vasculature shares common regulators, such as VNS and HD-ZIPIII transcription factors (*5*, *9*).

To understand the manner in which the AM initiation program is innovated, we identified *AtLAS* orthologous genes in *P. patens* and demonstrated that they are required for leaf midrib formation through specific mediation of leaf cell division. Notably, we found that *Arabidopsis las-101* mutant leaf axil cells also have reduced cell division. Promoting cell division by exogenous treatment with cytokinins restores both midrib formation and AM initiation in *Physcomitrium* and *Arabidopsis* mutants, respectively, implying an evolutionarily conserved cellular function of the AtLAS/PpLAS module. Together, our findings suggest that conserved molecular modules are co-opted during evolution and repetitively used by different lineages to create new structures.

RESULTS

P. patens LAS orthologs are highly expressed in leaves

Two orthologs of AtLAS were identified in the genome of *P. patens*, and their proteins share 43.6% (Pp3c6_16410, named PpLAS1) and 42.8% (Pp3c5_17790, PpLAS2) identity with AtLAS, respectively (fig. S1A). Phylogenetic analysis indicates monophyly of the bryophyte sequences, and the two *Physcomitrium* orthologs form one monophyletic clade (Fig. 1A and fig. S1B).

[1]College of Life Sciences, University of Chinese Academy of Sciences, Beijing 100049, China. [2]State Key Laboratory of Plant Genomics and National Center for Plant Gene Research (Beijing), Institute of Genetics and Developmental Biology, The Innovative Academy of Seed Design, Chinese Academy of Sciences, Beijing 100101, China. [3]State Key Laboratory of Protein and Plant Gene Research, Peking-Tsinghua Center for Life Sciences, Center for Quantitative Biology, School of Life Sciences, Peking University, Beijing 100871, China.
*Corresponding author. Email: yingwang@ucas.ac.cn (Y.W.); yuling.jiao@pku.edu.cn (Y.J.)
†These authors contributed equally to this work.

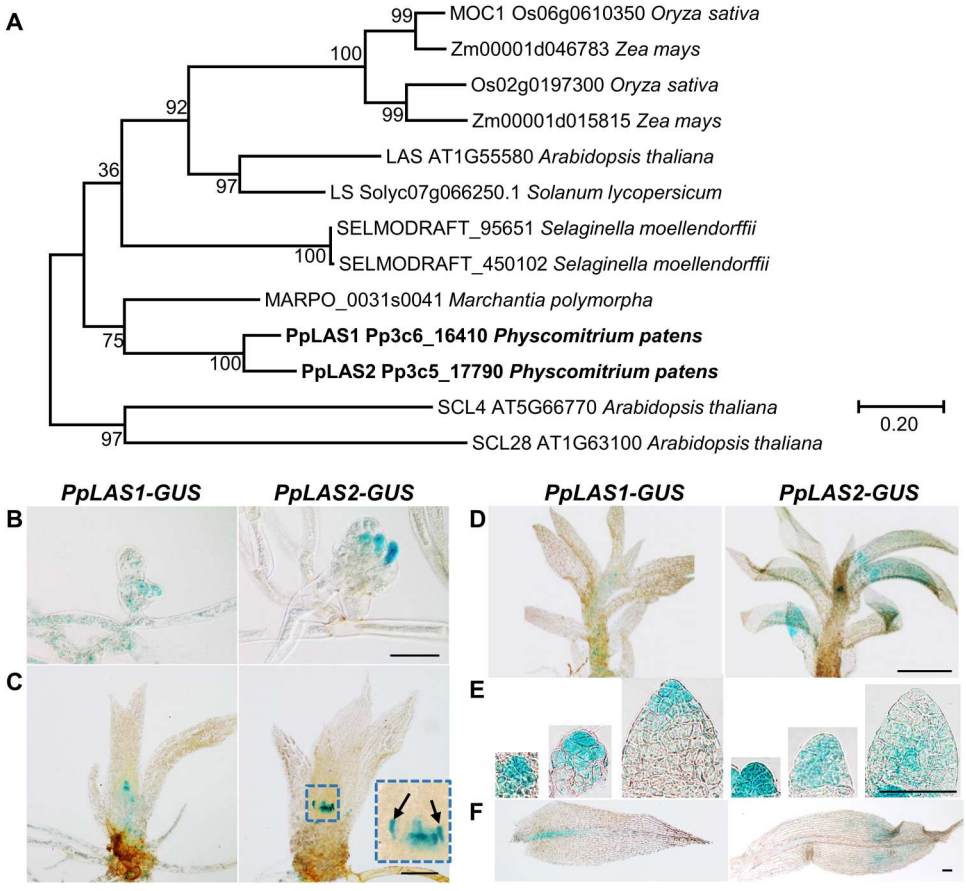

Fig. 1. Basic information about PpLAS orthologs and their expression patterns. (**A**) Phylogenetic analysis of LAS orthologs and their closest *Arabidopsis* paralogs (SCL4 and SCL28) as the outgroup. Full-length amino acid sequences of the proteins were aligned by ClustalW, and a phylogenetic tree was constructed using the maximum-likelihood method with MEGA7. Numbers at the branch nodes represent the confidence level of 2000 bootstrap replications. For each sequence, the gene name (where available), gene ID (Phytozome database), and species name are shown to the right of the tree branches. Scale bar represents a distance of 0.2 substitutions per amino acid position. (**B** to **F**) GUS expression patterns in young and mature vegetative gametophores of transgenic lines *PpLAS1-GUS* (left) and *PpLAS2-GUS* (right): gametophore buds (B), young gametophores with 4 to 5 visible leaves (C), gametophores with more than 12 leaves (D), newly emerged leaves from the gametophore tip (E), and mature adult leaves (F). Inset in (C) denotes the hair cells expressing *PpLAS2-GUS*. Scale bars, 100 μm (B, C, and F), 1 mm (D), and 50 μm (E).

Both *PpLAS* genes are expressed in both protonemata and gametophores of the haploid gametophyte, as well as in the tissues of the diploid sporophyte. To further analyze the precise localization of PpLAS proteins, we generated multiple independent lines of protein fusions with β-glucuronidase (GUS) (fig. S2), which are morphologically indistinguishable from the wild type. Comparable signals were obtained for multiple independent GUS lines of each gene.

During vegetative growth, both *PpLAS1* and *PpLAS2* are expressed in protonemata, including chloronemata and caulonemata (fig. S3, A and B), but are not detectable in rhizoids (fig. S3C). These genes are also expressed in developing gametophores (Fig. 1, B and C), as well as in mature gametophores with a number of leaves (Fig. 1D), and their expression persists in leaves since early stages (Fig. 1E). During leaf development, *PpLAS1* and *PpLAS2* expression patterns show discernible differences. *PpLAS1-GUS* becomes gradually restricted in the central region that subsequently develops into the midrib (Fig. 1F). By contrast, *PpLAS2-GUS* is highly expressed in the apical half of mature leaves (Fig. 1F) and in hair cells (Fig. 1C, inset, and fig. S3F). During reproductive growth, *PpLAS1* and *PpLAS2* also show distinct expression patterns. *PpLAS1* is expressed at the tip of the developing archegonium and gradually becomes undetectable in archegonia older than stage 7 (fig. S3D) (*10*). With respect to *PpLAS2*, GUS activity is prominent in the egg cell cavities of archegonia (fig. S3D). Their expression in antheridia is much weaker than that in archegonia; *PpLAS1* has a low expression level in developing antheridia, while *PpLAS2* expression is undetectable (fig. S3D). In the sporophytic generation, both *PpLAS1* and *PpLAS2* are expressed in the basal half of the embryos and the seta of developing and mature sporophytes (fig. S3E).

PpLAS affects midrib specification and leaf expansion

To investigate their functions, we generated single and double loss-of-function mutants using a gene-targeting approach (fig. S2) (*11*, *12*). All the single insertional knockout mutant lines generated through this approach display no discernible developmental defects during the vegetative growth stages. However, in the double-knockout *pplas1*-KO *pplas2*-KO (hereafter referred to as double-KO or D-KO in figures) lines, leaf expansion is significantly

reduced with respect to both length and width, with width being affected to a higher extent than length (Fig. 2, H and I, and fig. S4), although the overall morphologies and sizes of the mutant spot culture are comparable to those of the wild type (fig. S5). As a result, the aspect ratio (the ratio of length to width) is increased to 124% of that of the wild type in the double-KO line (Fig. 2J and table S1). The leaf base contains more elongated cells in the double-KO mutants (Fig. 2G, fig. S4, and insets in table S1), indicating that cells might quit division at earlier time points in the double-KO than in wild type. Midrib formation is fully abolished in the leaves of the double-KO mutant (Fig. 2, A to F, and table S2), but not in either single-KO mutant (table S2), suggesting that *PpLAS1* and *PpLAS2* redundantly affect midrib formation. To examine water transport in the double-KO mutant, excised leaves were soaked in Evans blue dye, which was absorbed from the cutting edges of the leaf base and traveled up the midrib (*5*). The dye travel distance was greatly reduced in the mutants as compared with the wild type, implicating deficient water transport in the mutants (fig. S6). Reflecting the deficiency in water transport, in the double-KO mutant, the angles between leaves and stems are smaller, and the leaves are slightly crinkly and more prone to wilting under relatively low humidity (fig. S7), similar to aquaporin mutants (*13*). Cross sections of adult leaves verified that the midrib, as a multistratose water-conducting tissue in the wild type (Fig. 2, B and C), is almost totally missing in the mutants (Fig. 2, E and F). We also generated CRISPR-Cas9–based *PpLAS* mutants to confirm their functions in midrib formation (fig. S8 and table S2). Notably, in the various truncation mutants that we obtained, most double mutants of both *PpLAS1* and *PpLAS2* lack midribs, while most single mutants retain the functional midribs, with the exception of the two dominant-negative truncation lines for *PpLAS2*, *pplas2-2* and *pplas2-3* (fig. S8; please also refer to Supplementary Text and fig. S21), which have also lost midrib formation capacity (figs. S4 to S6 and S8 and table S2). Together, *PpLAS1* and *PpLAS2* work in a redundant fashion to promote midrib formation. Since most double mutants consistently display similar developmental defects (table S2), we mainly focused on the double-KO mutant line for subsequent detailed phenotypic analyses.

PpLAS promotes cell division

To analyze the dynamics of midrib formation, we dissected the gametophore tip and closely observed the cell arrangement in early developing leaves (Fig. 3A). In wild-type young leaves with a width of <50 μm, elongated wedge-shaped precursor cells align in

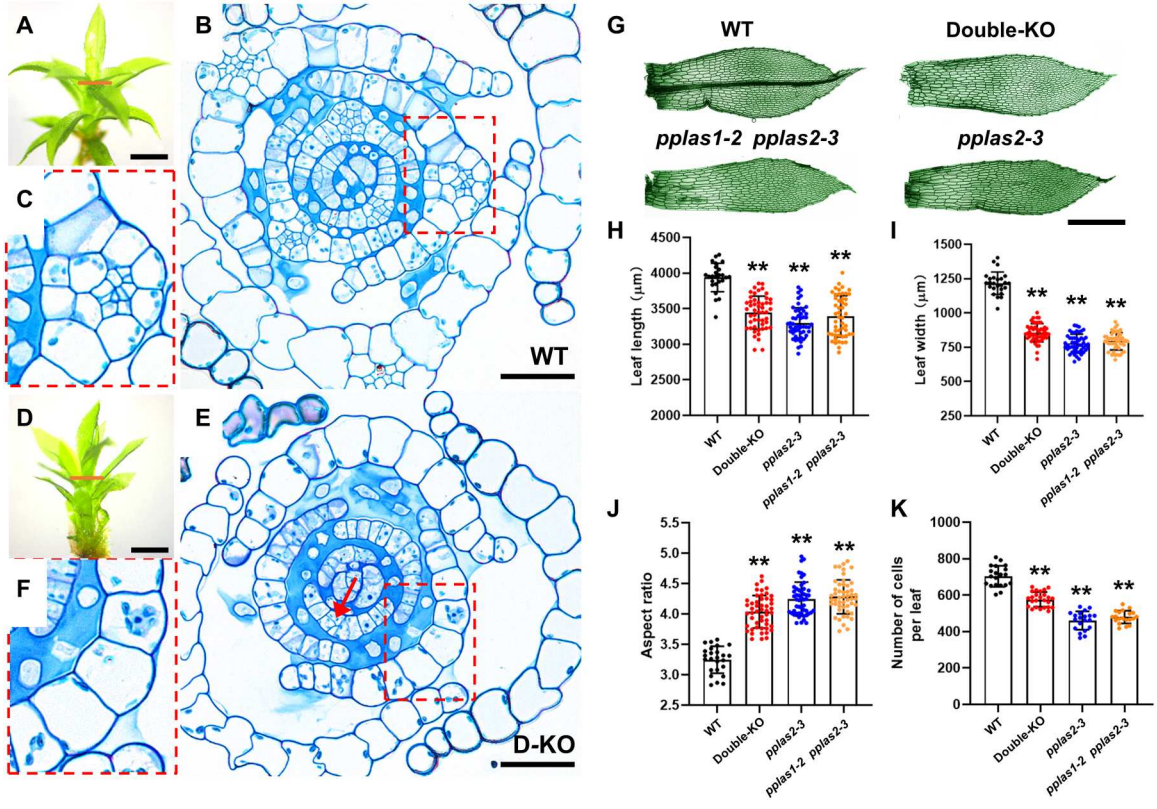

Fig. 2. *Physcomitrium pplas* mutants are defective in midrib formation and leaf expansion. (**A** and **D**) Gametophores (21 days old) of wild type (WT) (A) and double-KO mutant (D-KO) (D). The orange line in each figure represents the sectioning position shown in (B) or (E). Scale bars, 1 mm. (**B** and **E**) Transverse semithin sections of WT (B) and D-KO (E) stained with TBO for cell outlines. The red arrow in (E) indicates the occasional double cell layer observed in the cross sections in D-KO. Scale bars, 50 μm. (**C** and **F**) Enlarged insets of (B) and (E), respectively. (**G**) Leaf morphologies of 21-day-old WT (top left), double-KO (top right), *pplas1-2 pplas2-3* mutant (bottom left), and *pplas2-3* (bottom right). Leaves between L_{10} and L_{14} were used for quantification in (H) to (K). Scale bar, 1 mm. (**H**) Diagram showing the statistics of leaf (phyllid) lengths among different genotypes. (**I**) Diagram showing the statistics of leaf (phyllid) widths among different genotypes. (**J**) Diagram showing the statistics of leaf (phyllid) aspect ratios among different genotypes. (**K**) Diagram showing the statistics of leaf (phyllid) cell numbers among different genotypes. $^{**}P < 0.001$, by Student's *t* test ($n \geq 20$).

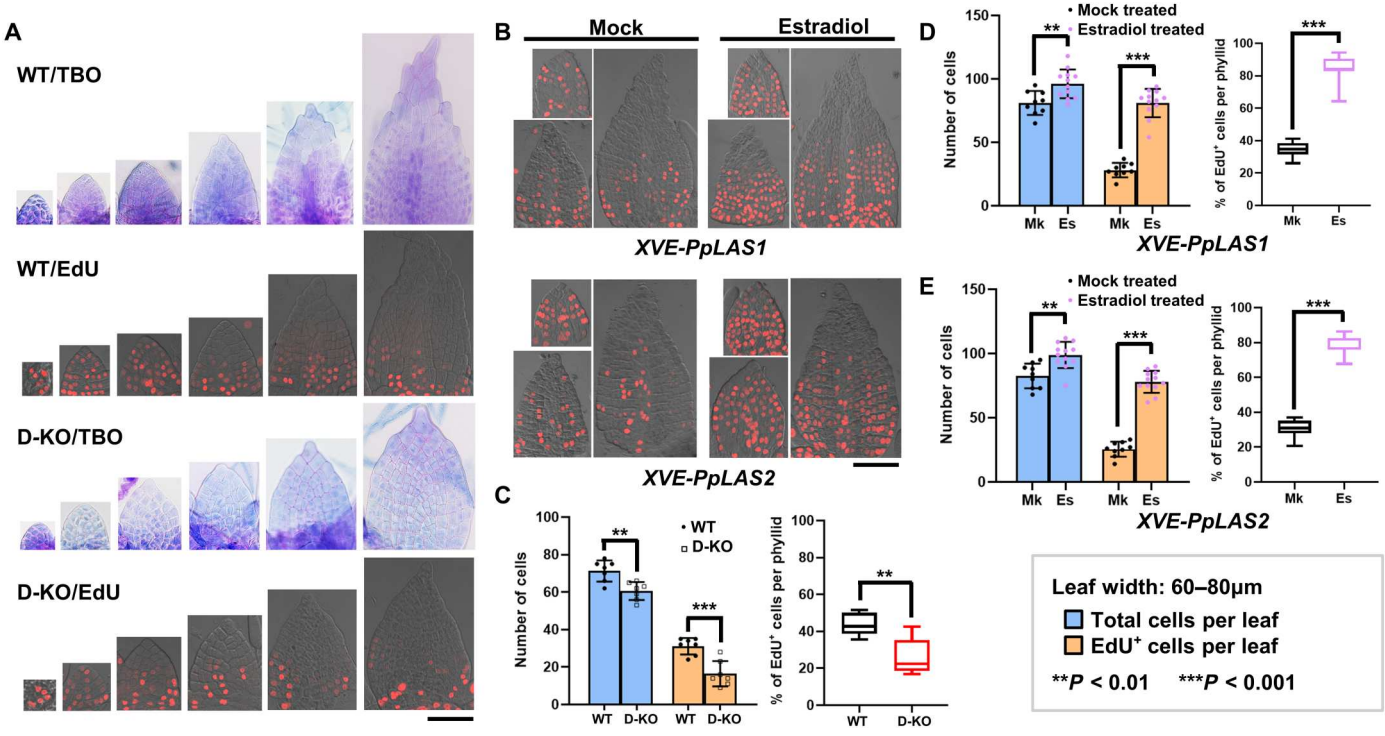

Fig. 3. *Physcomitrium pplas* mutants have reduced cell division, and *PpLAS* overexpression lines have enhanced cell division. (**A**) TBO-stained (first and third rows) and EdU/Alexa555-stained (4 hours for the smallest leaves and 12 hours for other leaves, second and fourth rows) young leaves from the 21-day-old gametophore tips of wild-type and double-KO (D-KO) mutant plants. Genotypes and staining reagents are indicated at the top left corner of each row. (**B**) EdU/Alexa555-stained (12-hour) young leaves from the gametophore tips of mock-treated (left column) and β-estradiol–treated (right column) *XVE-PpLAS1* (top row) and *XVE-PpLAS2* (bottom row). Genotypes are indicated at the bottom, and treatment modes are indicated at the top. (**C**) Quantitation of the total cell number (blue) and EdU$^+$ cell number (orange) in wild-type (WT) and double-knockout (D-KO) leaves (left graph) and of the percentage of EdU$^+$ cells per leaf (right graph). (**D**) Quantitation of the total cell number (blue) and EdU$^+$ cell number (orange) of mock-treated and β-estradiol–treated *XVE-PpLAS1* leaves (left) and of the percentage of EdU$^+$ cells per leaf (right). (**E**) Quantitation of the total cell number (blue) and EdU$^+$ cell number (orange) of mock-treated and β-estradiol–treated *XVE-PpLAS2* leaves. Scale bars, 50 μm. $^{**}P < 0.01$ and $^{***}P < 0.001$, by Student's *t* test ($n \geq 6$).

the middle along the apical-basal axis and will further develop into midribs (Fig. 3A, WT TBO, and figs. S9 and S10), suggesting that midribs start to form early in leaf development. By contrast, in the double-KO mutants, the elongated premidrib cells are totally missing, and the cells in the middle are indistinguishable from other blade cells (Fig. 3A, D-KO TBO, and figs. S9 and S10), suggesting that leaf cells fail to differentiate into premidrib cells in *pplas* mutants.

Since the leaf cell number is also significantly decreased in the midribless mutants (Fig. 2K), the distinct cell arrangement may be attributed to reduced cell division activity in *pplas* mutants. To test this hypothesis, we profiled the cell division activity in early leaves of both wild type and double-KO using 5′-ethynyl-2′-deoxyuridine (EdU), which can only be incorporated into genomic DNA during the S phase of the mitotic cycle (*14*, *15*). Our results suggest that the frequency of leaf cell division is significantly reduced in *pplas* mutants, as indicated by the percentage of EdU-positive cells in early developing leaves (Fig. 3C). Wild-type young leaves have a number of actively dividing cells (Fig. 3A, WT EdU). As a comparison, double-KO mutant leaf cells do not have as many actively dividing cells (Fig. 3A, D-KO EdU) during the initiation stage of midrib formation, which is accomplished when leaves reach the length of 160 μm (fig. S10), suggesting that *PpLAS1* and *PpLAS2* are necessary to maintain mitotic activity during leaf development.

Next, to further test whether *PpLAS1* and *PpLAS2* can promote cell division, we overexpressed either *PpLAS1* or *PpLAS2* and examined leaf development. By using the XVE (LexA-VP16-ER) system (*16*), we generated ubiquitously expressed β-estradiol–inducible overexpression lines (fig. S11). We also developed a detached Gametophore Culture (deGC) methodology to synchronize leaf emergence (fig. S12; please also see Materials and Methods for details). After β-estradiol treatment, newly formed *XVE-PpLAS1* and *XVE-PpLAS2* leaves have evidently formed substantially wider multistratose midribs than mock-treated leaves (Fig. 4, A and B). On occasion, ectopic multistratose rib-like structures can also be observed in blade areas that are one cell thick in the wild type (insets, Fig. 4, A and B). Microscopic analysis of the leaf cross sections suggests that these rib-like structures have multiple layers of cells (Fig. 4, C and D). The cell number in these ribs is also increased (Fig. 4, E and F), supporting the notion that *PpLAS* overexpression promotes cell division. In other cases, multiple cell layers are observed throughout the leaves, suggesting that ectopic *PpLAS* expression induces systematic cell overproliferation (Fig. 4, C and D). Analysis of EdU incorporation confirmed that mitotic activity is much higher in β-estradiol–treated lines than in mock controls (Fig. 3, B, D, and E). Together with the compromised cell proliferation in *pplas* mutants, these results suggest that *PpLAS* genes promote midrib formation by enhancing cell proliferation.

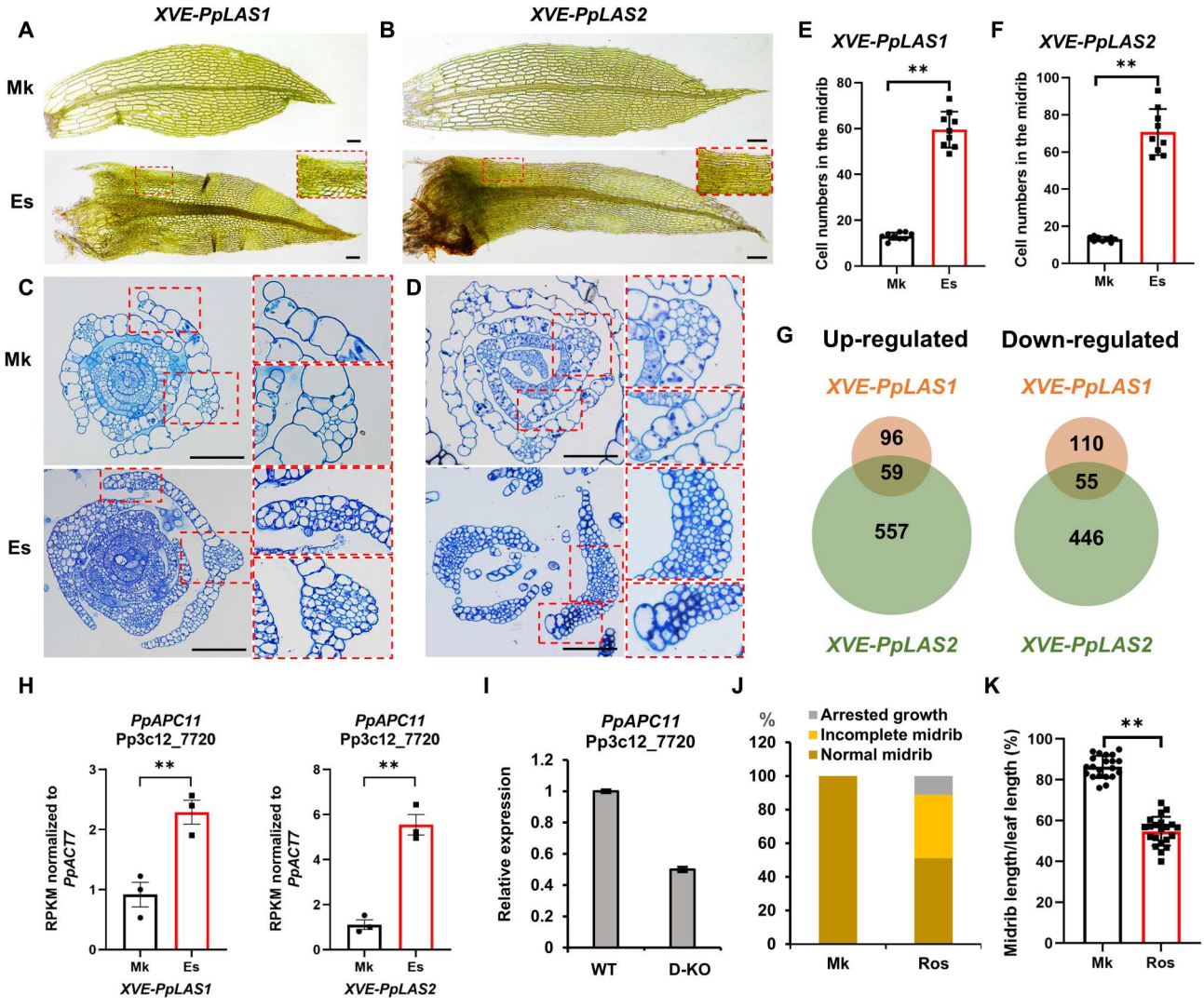

Fig. 4. *PpLAS1* and *PpLAS2* overexpression promotes midrib formation. (**A**) Mock-treated (Mk, top) and β-estradiol–treated (Es, bottom) *XVE-PpLAS1* leaves. (**B**) Mock-treated (Mk, top) and β-estradiol–treated (Es, bottom) *XVE-PpLAS2* leaves. The blue arrows in (A) and (B) indicate rib-like structures. (**C**) TBO-stained semithin sections of mock-treated (Mk, top) and β-estradiol–treated (Es, bottom) *XVE-PpLAS1* plants. Magnified insets are shown on the right. (**D**) TBO-stained semithin sections of mock-treated (Mk, top) and β-estradiol–treated (Es, bottom) *XVE-PpLAS2* plants. Magnified insets are shown on the right. (**E**) Quantitation of the total cell number per midrib in (A). (**F**) Quantitation of the total cell number per midrib in (B). (**G**) Venn diagram of the genes up-regulated (left) and down-regulated (right) by *PpLAS1* (orange) and *PpLAS2* (green) overexpression. (**H**) RPKMs (Reads Per Kilobase per Million mapped reads) of *PpAPC11* (Pp3c12_7720) normalized to *PpACT7* (Pp3c3_33410) in RNA-seq of β-estradiol–treated *PpLAS1* and *PpLAS2* overexpression lines compared to mock-treated control. (**I**) RT-qPCR results for *PpAPC11* (Pp3c12_7720) in WT and the double-KO (D-KO) mutants. (**J**) Composite bar graph showing the percentage of leaves with normal or abnormal midrib formation in mock-treated (Mk) and roscovitine-treated (Ros) WT plants. At least 45 gametophores were used for each treatment. (**K**) Quantitation of the average midrib intactness following mock (Mk) and roscovitine (Ros) treatment, indicated by the ratio of midrib length over leaf length. Scale bars, 100 μm. $^{**}P < 0.01$, by Student's *t* test. $n = 9$ (E and F) and $n = 20$ (J).

Ectopic expression of PpLAS up-regulates the cell cycle regulator APC11

To identify potential target genes that function downstream of *PpLAS* and elucidate the molecular mechanism underlying midrib formation, we performed RNA sequencing (RNA-seq) analysis of the β-estradiol–inducible *XVE::PpLAS1* and *XVE::PpLAS2* plants. In total, 114 common downstream targets of *PpLAS1* and *PpLAS2* were identified (Fig. 4G and table S3). Among them, we found the gene Pp3c12_7720 (hereafter referred to as *PpAPC11*), encoding anaphase-promoting complex (APC) subunit 11, to be substantially up-regulated by *PpLAS* overexpression (Fig. 4H). We subsequently evaluated its expression in the *pplas1 pplas2* double-KO mutant and found it to be significantly decreased (Fig. 4I). This suggests that *PpAPC11* might be a potential target of *PpLAS* genes. The roles of PpAPC11 in cell proliferation and midrib formation await further investigation.

Promotion of the cell cycle restores midrib formation to *pplas* mutants

Cytokinin is known to promote cell proliferation (*17*–*19*); therefore, to evaluate whether promoting cell division can restore midrib formation, we treated the *pplas1 pplas2* double-KO mutants with kinetin, a cytokinin analog. We observed thick midrib-like structures (Fig. 5A) reminiscent of those induced by *PpLAS*

overexpression (Fig. 4, A and B), and the leaf width is also greatly increased (Fig. 5A). Analysis of cross sections of the treated leaves revealed that multistratose bundle-like structures form after kinetin treatment (Fig. 5B). However, in comparison with the wild-type leaf midribs, more cells are induced by kinetin and the cell walls are much thinner (fig. S13), suggesting that a secondary cell wall may not form efficiently. No signs of mature hydroids and stereids, such as cytoplasmic depletion and cell wall thickening, are detectable (fig. S13). Cells located at the position of hydroids retain cellular contents (fig. S13). In addition, kinetin-treated mutant leaves do not efficiently transport Evans blue dye (fig. S14), indicating that these midrib-like structures are not fully functional. These results suggest that active cell division is necessary but not sufficient for midrib formation, and additional essential functions are exerted by *PpLAS* genes.

In wild-type plants, juvenile leaves form at the basal positions of gametophores, lack intact midribs, and have a different morphology from that of adult leaves (fig. S15A) (*7*, *9*). To test whether such distinctions can be attributed to different cell division activities, we treated gametophores with kinetin from the bud stage and dissected the two most basal leaves. By analyzing 100 gametophores, we found that kinetin treatment can also promote multistratose midrib

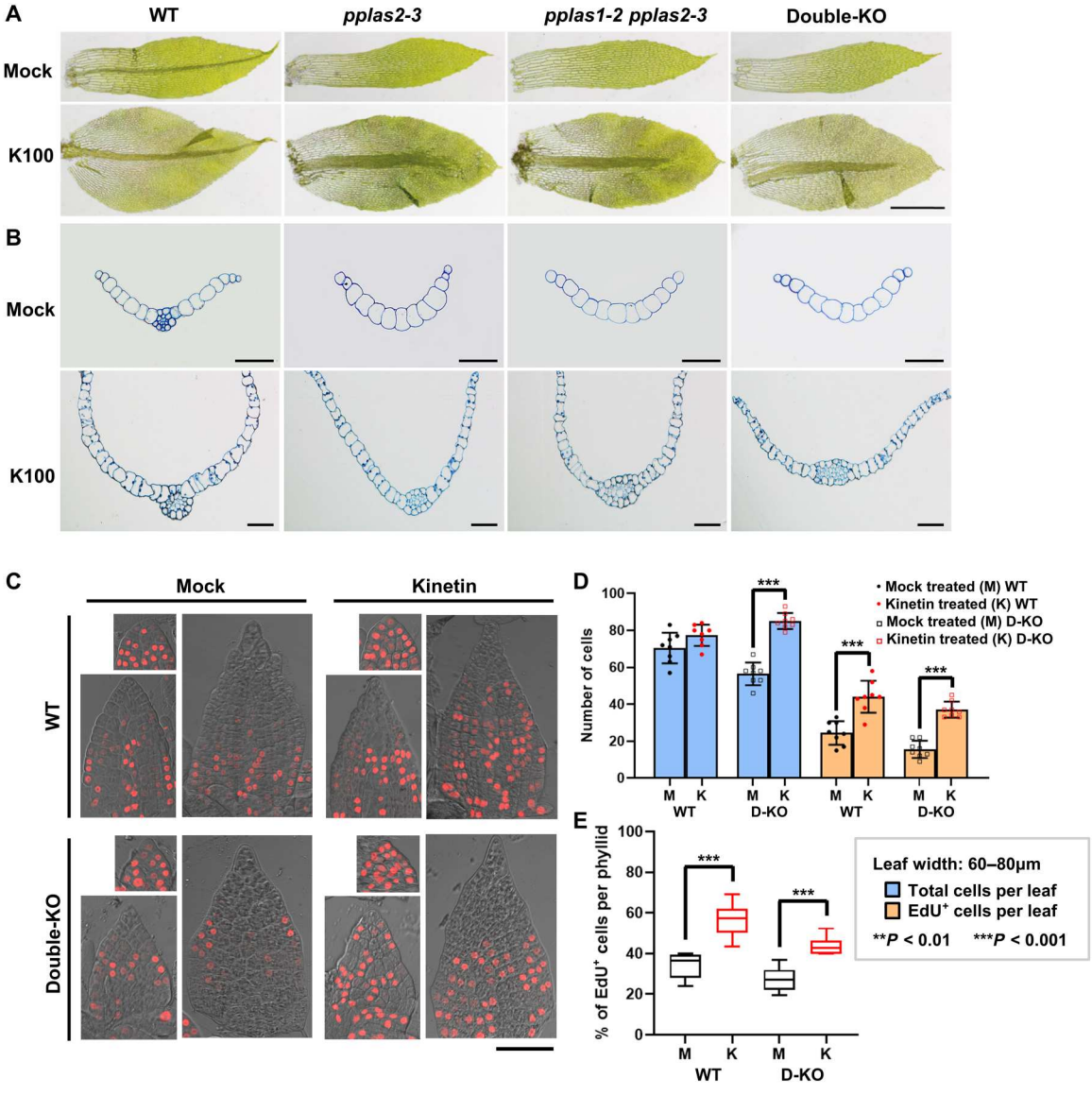

Fig. 5. Promotion of cell division by cytokinin partially rescues midrib defects in *Physcomitrium pplas* mutants. (**A**) Mock-treated (top) and kinetin-treated (100 μg/L; K100, bottom) wild-type (WT), *pplas2-3*, *pplas1-2 pplas2-3*, and double-KO mutant leaves. Genotypes are indicated at the top of the corresponding panel. (**B**) TBO-stained semithin transverse sections of mock-treated (top) and kinetin-treated (100 μg/L; K100, bottom) WT, *pplas2-3*, *pplas1-2 pplas2-3*, and double-KO leaves. Genotypes are indicated at the top of the corresponding panel. (**C**) EdU/Alexa555-stained (12-hour) young leaves from the gametophore tips of mock-treated (left column) and kinetin-treated (right column) WT (top row) and double-KO mutant (bottom row). Genotypes are indicated to the left, and the treatment modes are indicated at the top. (**D**) Quantitation of the total cell number (blue) and EdU$^+$ cell number (orange) of wild-type (WT) and double-knockout (D-KO) leaves following mock (M) and kinetin (K) treatment. (**E**) Quantitation of the percentage of EdU$^+$ cells per leaf of wild-type (WT) and double-knockout (D-KO) leaves following mock (M) and kinetin (K) treatment. Scale bars, 1 mm (A), 100 μm (B), and 50 μm (C). $^{**}P < 0.01$ and $^{***}P < 0.001$, by Student's *t* test ($n > 6$).

formation in the second juvenile leaves (fig. S15, B and C). Although the first leaves at the most basal position still fail to form midribs under kinetin induction, the cells in the central region are elongated and can be clearly distinguished from other leaf cells (fig. S15B). Furthermore, kinetin treatment greatly enhances blade cell division in the most basal juvenile leaves, resulting in leaf expansion, and the shape of the basal leaves resembles that of adult leaves (fig. S15). This finding further confirms that promoting cell division induces midrib formation.

Moreover, to assess the effects of prohibited cell division on midrib formation, we treated plants with roscovitine, a cyclin-dependent kinase inhibitor (*20*). We found that in comparison with mock-treated plants, those treated with roscovitine are retarded in overall growth and have a much shorter stature. In addition, roscovitine-treated leaves contain fewer but larger cells, and midrib formation is significantly disrupted (Fig. 4, J and K, and fig. S16).

AtLAS promotes cell division in the leaf axil

Arabidopsis las-101 mutants fail to form AMs during vegetative growth (Fig. 6B, as compared with wild-type plants in Fig. 6A) (*1*). However, because of the unique morphology of the saddle-shaped boundary zones and the tightly packed cells within these zones (*21*, *22*), it remains unsolved which cellular processes are regulated by LAS to affect AM initiation. To answer this question, we first compared the cell morphology of the Col-0 wild type (Fig. 6C) and *las-101* mutants (Fig. 6D) within the leaf axil where AM is initiated. We analyzed P11, which denotes the 11th youngest leaf, when AM initiation starts (*23*), and found that the cells in *las-101* P11 leaf axils are substantially fewer and larger than those in the wild-type leaf axils (Fig. 6I). Subsequently, we applied the EdU staining assay to directly monitor cell division. More EdU incorporation can be detected in the wild-type leaf axils than in the *las-101* mutant leaf axils (Fig. 6, E and F), confirming that cell division is reduced in the mutant. The region lacking cell division is wider than the *AtLAS* expression region, suggesting that *AtLAS* may regulate cell division in a non–cell-autonomous fashion. Together, our results show that *AtLAS* promotes cell division in a manner similar to *PpLAS*. *AtLAS* expression is not detected in the vasculature (*1*). Consistently, we found that vasculature development in *las-101* is comparable to that in the wild type, without detectable defects (fig. S17).

We next examined whether promoting cell division can rescue *Arabidopsis* AM initiation defects in *las-101*. To this end, we isolated P_8 to P_{10} and treated the leaves with kinetin or 6-benzylaminopurine (BAP), a synthetic cytokinin species. We found that treatment with either kinetin or BAP is able to restore AM formation (Fig. 6, G, H, and J, and fig. S18). After mock treatment, only 53% of *las-101* leaves form AMs. By contrast, 96% of *las-101* leaves form AMs following treatment with kinetin (200 μg/L; table S4). Similar results were obtained with BAP treatment (fig. S18). These results suggest that sufficient cell division is crucial for AM initiation. Together, our findings reveal that the compromised mitotic activity accounts for the defects in AM initiation observed in the *las-101* mutants.

Partial complementation of *Arabidopsis* las mutant by PpLAS

Although mosses and seed plants diverged >400 million years ago (*24*), we attempted to evaluate whether *PpLAS* can replace the function of *AtLAS*. We fused the ~3000–base pair regulatory sequence upstream of the start codon of *AtLAS* to the coding sequence of *PpLAS2* and *Venus* and then introduced this into the homozygous *las-101* mutant (Fig. 6K). Among the 14 independent transgenic lines that we obtained, at least 4 have mild restoration of AM initiation capacity in the youngest rosette leaves (Fig. 6K); however, the leaf-stem and branch-stem fusion phenotype was not rescued.

We also attempted to replace *PpLAS* with *AtLAS*. To this end, we replaced the disrupted *PpLAS2* coding sequence region in the dominant-negative *pplas2-3* mutant with the *AtLAS* coding sequence. However, midrib formation defects were not restored in a total of 15 independent transgenic lines (fig. S19), suggesting that AtLAS is not equivalent to PpLAS2 and interferes with PpLAS1 function such that the transgenic lines have a stronger phenotype than *pplas2*-KO plants. Together, these results demonstrate that *PpLAS2* can partially replace *AtLAS* but not vice versa.

Most GRAS family genes encode transcription factors (*4*). To test whether the midrib-promoting function relies on the transcriptional activity of PpLAS proteins, we replaced the endogenous *PpLAS2* coding sequence with a fusion of *PpLAS2* to the glucocorticoid receptor (GR) and a 3×hemagglutinin (HA) tag in the background of the *pplas1-3* mutant (fig. S20A). GR retains PpLAS2 in the cytosol unless treated with dexamethasone (Dex), which induces the translocation of PpLAS2-GR-3×HA to the nucleus. Due to the functional redundancy between PpLAS1 and PpLAS2, *pplas1-3* mutant has normal leaves with intact midribs (table S2). By contrast, in the resulting *pplas1-3 PpLAS2-GR-3×HA* plants, midrib formation is greatly compromised without Dex treatment (fig. S20B), mimicking the double mutants (Fig. 3G and tables S1 and S2). As a comparison, Dex treatment greatly restores midrib formation to *pplas1-3 PpLAS2-GR-3×HA* plants (fig. S20). Our results suggested that PpLAS2 must function in the nucleus to promote midrib formation and further confirmed that PpLAS2 works in a redundant fashion with PpLAS1.

DISCUSSION

Major innovations in plant body plans and anatomical structures define different lineages during evolution. It has been proposed that reusing existing regulatory modules could facilitate these innovations (*5*, *25*, *26*); however, the underlying molecular mechanisms remain largely unknown. In the present study, we demonstrate that the LAS regulatory module, which promotes cell proliferation, has been reused during evolution. In mosses, this module is involved in the formation of the leaf midrib, a water-conducting and supporting tissue with a similar function to that of vascular tissue in tracheophytes. Our results demonstrate that LAS is a key determinant of moss midrib formation, but not of *Arabidopsis* vascular tissue formation (fig. S17), suggesting that the two types of water-conducting tissues use different regulatory modules. On the other hand, LAS is used for AM initiation in seed plants. AMs enable seed plants to use lateral branching in place of terminal branching, which is commonly seen in Lycopsida and ferns, to efficiently occupy space and adapt to changing environments (*27*). Together, these findings provide a notable case, in which a conserved molecular module is reused during evolution to innovate distinct anatomical structures. GRAS family genes were acquired by the common ancestor of Zygnematophyceae and embryophytes through horizontal gene transfer from soil-residing bacteria (*4*). This suggests that they may play essential roles in plant adaptation to environmental challenges on land, such

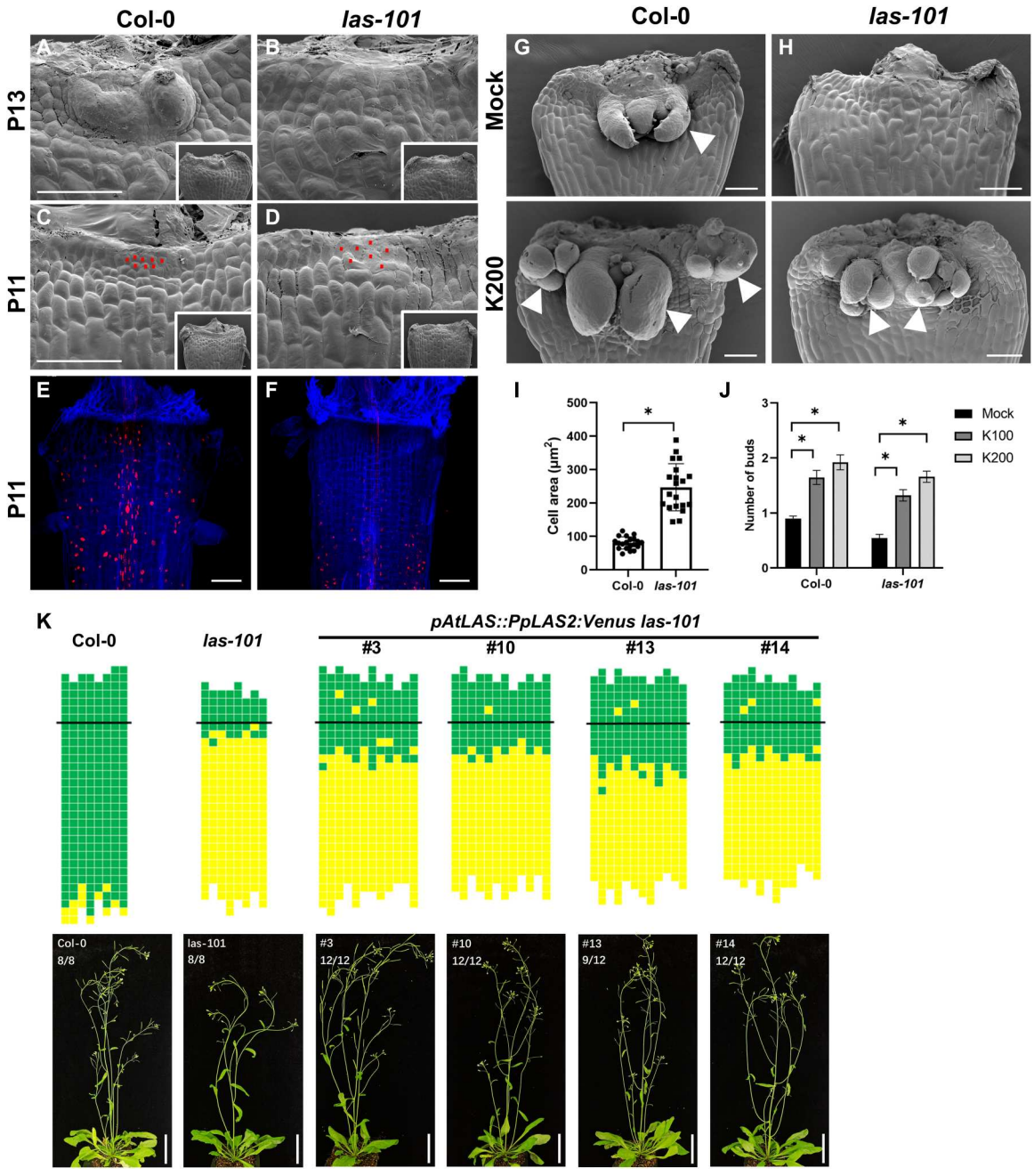

Fig. 6. *Arabidopsis las-101* mutants have comparably reduced cell division, which can be partially rescued by cytokinin treatment and expression of *PpLAS2*. (**A** to **D**) Scanning electron microscopy (SEM) images of P13 (top) and P11 (bottom) leaf axils: (A) wild type (Col-0) P13; (B) *las-101* P13; (C) Col-0 P11; (D) *las-101* P11. Red dots in (C) and (D) indicate the cells used to calculate the average cell area for the graph in (I). Scale bars, 100 μm. (**E** and **F**) EdU/Alexa555-stained P11 leaf axils of Col-0 (E) and *las-101* (F). Scale bars, 100 μm. (**G** and **H**) SEM images of mock-treated (top) and kinetin-treated (200 μg/L; bottom) leaf axils of wild Col-0 (G) and *las-101* (H). White triangles indicate axillary buds. Scale bars, 100 μm. (**I**) Average area of selected leaf axil cells [illustrated by red dots in (C) and (D)] from Col-0 and *las-101*. Three samples from Col-0 and *las-101* were used for quantitation. *$P < 0.01$, by Student's *t* test ($n > 20$). (**J**) Quantitative graph for the number of axillary buds per leaf of the WT and *las-101* following mock and kinetin (100 and 200 μg/L) treatment. *$P < 0.01$, by Student's *t* test ($n > 50$). (**K**) Diagrams of axillary bud formation in wild-type (Col-0), *las-101*, and various *proAtLAS::PpLAS2 las-101* lines. Top row: Each column represents a single plant, and each square represents one leaf axil. The black horizontal line represents the border between the youngest rosette leaf and the oldest cauline leaf. The bottom square represents the oldest rosette leaf axils, with progressively younger leaves above. Green indicates the presence of an axillary bud, and yellow indicates the absence of an axillary bud. Bottom row: Typical plant architecture of Col-0, *las-101*, and various *proAtLAS::PpLAS2 las-101* lines. Genotypes are indicated above the corresponding panel. Scale bars, 5 cm.

as evolving midribs for support and water transport in bryophytes and boundary regions to harbor and protect new stem cell niches in seed plants (*21*, *22*). *LAS* genes encode transcription factors, which likely promote multiple downstream pathways involved in midrib initiation and subsequent development. Their target gene regulatory network remains to be identified and unveiled in future studies. Such analysis holds promise to elucidate responsible executors for different aspects of midrib development.

Although AtLAS does not notably affect vascular development (this study), other GRAS family transcription factors do. The founding members of GRAS family, SCARECROW (SCR) and SHORTROOT (SHR), as well as SCARECROW-LIKE 23 (SCL23), were reported to control vascular bundle sheath formation (*28*), probably also through regulation upon cell division. Previous studies have also shown that VND/VNS transcription factors are commonly used by mosses and flowering plants to promote water-conducting cell specification in that they promote programmed cell death in moss hydroids and angiosperm tracheids to facilitate water transport (*5*, *26*, *29*). These together suggest that the formation of the bundle-like water-conducting tissues involves regulators of similar functions, such as promoting cell proliferation or promoting cell death. Nevertheless, these regulators are not necessarily conserved across all the species through evolution. Instead, members with similar functions from the same GRAS family might be recruited differentially. Given that leaves of mosses and tracheophytes, despite their planar structure and similar photosynthetic functions, have drastically different evolutionary origins, it is not unexpected that they evolved to use diverse proteins within the same family to achieve similar morphological and functional outcomes.

Our findings also highlight a cryptic similarity between water-conducting tissues and AM. Although these two types of structures are morphologically different and anatomically separated, LAS-promoted cell proliferation appears to be commonly required during their early specification. Despite the downstream gene regulatory networks of LAS remaining largely unresolved, HD-ZIPIII transcription factors likely play key roles. In *Physcomitrium*, ectopic expression of miR166, which targets HD-ZIPIII genes, causes compromised midrib formation (*9*). Similarly, mutations in *Arabidopsis REVOLUTA* (*REV*), encoding an HD-ZIPIII transcription factor, cause AM initiation defects as well as vascular and other developmental defects (*1*, *30*, *31*). *REV* expression is regulated by *AtLAS* (*1*), which may also hold true in *Physcomitrium*. Further investigation on LAS-REV module and the roles of REV in midrib formation is warranted to reveal more intriguing connections between mosses and tracheophytes. The evolutionarily conserved regulatory loop is reminiscent of the genetic interactions between *Class I KNOX* genes (*MKN2* in *Physcomitrium* and *STM* in *Arabidopsis*) and cytokinin biosynthesis pathways, which together regulate seta foot elongation and shoot apical meristem indeterminacy in *Physcomitrium* and *Arabidopsis*, respectively (*32*–*34*).

Although it is believed that boundary regions generally have low mitotic activity (*22*), we show that localized active cell division is required for AM initiation, which is regulated by *AtLAS*. Two recent studies have shown that *Arabidopsis* SCL28, a GRAS family member and a close paralog of AtLAS, regulates cell cycle progression and functions to actively balance cell division and cell growth (*35*, *36*). In addition, SHR and SCR directly activate cyclin D and affect formative cell division in root apical meristems (*37*). The results of our study add a further line of evidence for the active involvement of GRAS family transcription factors in cell division.

Both *PpLAS1* and *PpLAS2* are expressed throughout the newly emerging leaves and are redundantly required for midrib initiation. Unlike *PpLAS2*, the expression of which persists throughout the leaves at later stages, *PpLAS1* becomes more pronounced at the leaf tip and gradually becomes more midrib specific (Fig. 1E). This could suggest that despite the redundancy between the two *PpLAS* genes in midrib initiation, they could have acquired functional divergence in subsequent development. For example, *PpLAS2* may be more important in division promotion and midrib initiation, while *PpLAS1* may be more important in midrib differentiation. In addition, PpLAS proteins were tagged to GUS, which may block intercellular movement. The observed GUS staining patterns could be narrower than those of PpLAS proteins. It remains an open and intriguing question whether PpLAS proteins are mobile and whether such mobility is of functional significance, in a similar fashion to SHR, which moves from the stele to the adjacent cell layer to up-regulate SCR and promote endodermis specification (*38*, *39*).

MATERIALS AND METHODS

Materials and growth conditions

Physcomitrium *plant growth*

All strains were derived from the Gransden wild-type strain of *P. patens* and were grown on BCDAT medium at 25°C under long-day conditions (16 hours of light and 8 hours of dark). BCDAT medium is composed of 1 mM $MgSO_4$, 1.84 mM KH_2PO_4 (pH 6.5), 10 mM KNO_3, 45 μM $FeSO_4$, trace element solution (0.22 μM $CuSO_4$, 10 μM H_3BO_3, 0.23 μM $CoCl_2$, 0.1 μM Na_2MoO_4, 0.19 μM $ZnSO_4$, 2 μM $MnCl_2$, and 0.17 μM KI), 5 mM ammonium tartrate, 1 mM $CaCl_2$, and 0.7% agar. Protonemal tissues for protoplast transformation were cultured on cellophane-overlaid BCDAT medium for 1 week. Phenotypic analyses were conducted using 28-day-old gametophores unless otherwise specified. To induce sporophytes, protonemal tissues were inoculated on ammonium tartrate–free BCD medium (0.4 mM KNO_3 instead) at 25°C under long-day conditions for 1 month and then transferred to 16°C under short-day conditions (8 hours of light and 16 hours of dark) for an additional 6 weeks. The cultures were irrigated every other week to facilitate fertilization (*35*).

Arabidopsis *plant growth*

Arabidopsis thaliana ecotype Columbia (Col-0) was used as the wild-type control. The *las-101* mutant (*1*) and *proAtLAS::PpLAS2-VENUS* transgenic lines were in the Col-0 background. For axillary bud counting, plants were grown under short-day conditions (8 hours of light and 16 hours of dark at 22°C) for 30 days and then under long-day conditions (16 hours of light and 8 hours of dark at 22°C) for 30 days to induce flowering.

Methods

Construction of transgenic plants

To generate the *pplas1-2*, *pplas2-2*, *pplas2-3*, and *pplas1-2 pplas2-3* mutants, single-guide RNA (sgRNA) sequences targeting *PpLAS1* and/or *PpLAS2* with the lowest off-target hits were selected according to the CRISPR software. Corresponding oligo pairs were annealed and inserted into the pBS-sgRNA vector [a gift from H. Chen (*40*)] to create sgRNA constructs. Subsequently, the Cas9

stable line was transformed with these sgRNA constructs, or the wild type was cotransformed with these constructs and the pHIZ2-Cas9 vector [a gift from H. Chen (*40*)] containing an antibiotic selection marker for hygromycin. Other CRISPR-Cas9–derived mutant alleles (table S2) were generated using the system developed by the Bezanilla group [ADDGENE, catalog no. 1000000151 (*41*)].

To generate the double-KO mutant line, two plasmids were created to disrupt or replace the genomic *PpLAS1* and *PpLAS2* sequences. A 3-kb genomic fragment including the first exon of *PpLAS1* was cloned into the vector pBJ36, and then a hygromycin resistance cassette was inserted into the first exon of *PpLAS1*. The resulting plasmid, with 1.5-kb upstream and 1.5-kb downstream sequences as the left and right homologous arms, respectively, was named *pBJ36-PpLAS1*-KO. Deletion of *PpLAS2* was performed by replacing the genomic regions with the antibiotic selection marker for G418 carried by pTN182. Approximately 1 kb of 5′ genomic sequence before the start codon of *PpLAS2* was cloned into pTN182, and then 1 kb of 3′ genomic sequence after *PpLAS2* was inserted into the site downstream of the G418 resistance cassette to obtain the *pTN182-PpLAS2*-KO vector. Both plasmids were linearized and cotransformed to generate the double-knockout line.

To construct the *PpLAS* overexpression lines, the coding sequences of *PpLAS1* and *PpLAS2* were amplified from *P. patens* total RNA by reverse transcription polymerase chain reaction (RT-PCR), respectively, inserted into the Not I/Asc I sites of the pENTR-PpU6p-sgRNA-L1L2 entry vector using T4 DNA ligase, and subsequently inserted into the Gateway destination vector pPGX8 that contains a hygromycin resistance cassette [a gift from M. Hasebe (*16*)] using the Gateway LR Clonase II enzyme. The generated plasmids were linearized with the restriction enzyme Pme I for gene targeting and then introduced into the wild-type plants. Overexpression lines were characterized by quantitative RT-PCR (RT-qPCR) analyses.

For the generation of gene reporter constructs, approximately 1 kb of 5′ genomic sequence before the stop codon of *PpLAS* was inserted into the plasmid pTN182, and then the gene coding for the GUS reporter was cloned downstream of the 5′ genomic fragments, generating in-frame fusions of each *PpLAS* gene and the reporter gene. Approximately 1 kb of 3′ genomic sequence downstream of the stop codon of *PpLAS* was also inserted into pTN182 carrying the above 5′ fragment. The generated plasmids were linearized and transformed into the wild-type plants.

To build the *proAtLAS::PpLAS2-VENUS* construct, the *PpLAS2* coding sequence and the *VENUS* sequence were sequentially cloned in-frame into the BJ36 vector containing the *AtLAS* promoter. The entire *proAtLAS::PpLAS2-VENUS* fragment was introduced into the binary vector pMOA36 (with spectinomycin resistance), which was used to transform *las-101* plants.

To generate the *PpLAS2-GR-3×HA* construct, approximately 1 kb of 5′ genomic sequence before the stop codon of *PpLAS2* was inserted into the plasmid pTN182, and then sequences encoding GR and a 3× HA tag were inserted downstream of the 5′ genomic fragments to generate in-frame fusions. Approximately 1 kb of 3′ genomic sequences downstream of the stop codon of *PpLAS2* were inserted downstream of the GR-3×HA sequences. The resulting *PpLAS2-GR-3×HA* vector was linearized and introduced into the *pplas1-3* mutant. The primers used in this study to generate constructs and transgenic lines are provided in table S6.

Physcomitrium *genetic transformation*

Moss transformation was performed according to the polyethylene glycol (PEG)–mediated protoplast transformation procedure, as described previously (*42*). For CRISPR-Cas9–mediated genome editing approach, circular sgRNA and Cas9 plasmids (each 10 μg) were used to cotransform the wild type. For endogenous gene targeting, 20 μg of plasmid DNA was linearized through restriction endonuclease digestion, purified, and used for each transformation. Protonemal tissues were grown on cellophane-overlaid BCDAT medium for 1 week and then collected for digestion using 0.5% cellulose and 0.15% macerozyme solution (in 8% mannitol) for 1 hour. The protoplast suspension was filtered through a 70-μm cell strainer (BD Falcon 352350) to remove cell wall debris. Protoplasts were collected by centrifugation for 4 min at 180*g*, resuspended, and washed twice with equivalent volumes of 8% mannitol. Following cell counting using a hemocytometer, protoplasts were resuspended in MMM solution [9.1% mannitol, 15 mM $MgCl_2$, and 1% MES (pH 5.6)] to achieve a final concentration of 1.5×10^6/ml. Plasmids or purified DNA (up to 30 μl) was mixed with 300 μl of protoplast suspension and 300 μl of PEG solution [0.1 M $Ca(NO_3)_2$, 10 mM tris (pH 8.0), 8% mannitol, and 40% PEG 6000] by gently tilting the tubes. The mixture was incubated at room temperature for 30 min, then diluted with 1.5 ml of W5 solution [2 mM MES (pH 5.6), 5 mM KCl, 125 mM $CaCl_2$, and 154 mM NaCl], and resuspended in 4 ml of PRMT medium (BCDAT medium with 6% mannitol, 0.4% agar, and 10 mM $CaCl_2$). A 2-ml aliquot of the protoplast suspension was plated onto each cellophane-overlaid plate containing PRMB medium (BCDAT medium with 6% mannitol, 0.7% agar, and 10 mM $CaCl_2$). Protoplasts were grown under standard conditions for 4 to 7 days before being transferred onto BCDAT plates supplemented with antibiotics for selection [Hyg (30 μg/ml) and G418 (25 μg/ml)]. Regenerated plants were grown for 2 weeks on selection medium and subsequently transferred to BCDAT plates lacking antibiotics for a further 2 weeks. For homologous recombination, plants were subjected to a second round of the selection process.

Leaf morphological characterization

Gametophores (21 days old) with almost the same number of leaves were selected for phenotyping the leaf morphology. Leaves among the 10th (L_{10}) to 14th (L_{14}) leaf were dissected from each gametophore and photographed using an Olympus BX60 microscope equipped with a Nikon DS-Ri1 camera. Quantitative measurements were undertaken using the ImageJ software. The leaf length was measured as the distance between the leaf base and tip along the midline of the leaf. The leaf width was determined by the maximal leaf width across the widest part of the leaf. The leaf aspect ratio was calculated by dividing the leaf length by the leaf width for each leaf. Data analysis and visualization were performed in GraphPad Prism 9. At least 30 leaves from eight individuals were chosen for quantification.

Quantitative RT-PCR analysis

RNA samples were extracted using the AxyPrep Multisource Total RNA Miniprep Kit (Axygen), and complementary DNA (cDNA) was synthesized using the TransScript One-Step gRNA Removal and cDNA Synthesis SuperMix (Transgene). RT-qPCR was performed using the KAPA SYBR FAST qPCR Kit (KAPA Biosystems) on a Bio-Rad CFX96 real-time detection instrument.

Semithin sectioning and transmission electron microscopy

Observation of leaf midribs by transmission electron microscopy was performed as previously reported, with some modifications (*5*, *43*). Gametophore leaves (21 days old) at the same position from the shoot tip were fixed overnight at 4°C in 0.05 M Pipes buffer (pH 7.0) containing 1.5% glutaraldehyde and 1.5% formaldehyde and subsequently fixed in 0.05 M Pipes buffer (pH 7.0) containing 2% OsO_4 for a further 2 hours in the dark at 4°C. After being rinsed three times with distilled water, the leaves were dehydrated in a graded ethanol series to 100% for 30 min each. The fixed samples were embedded in Spurr resin (Low Viscosity Spurr Formula Kit) and polymerized at 65°C for 16 hours. For light microscopy, 5 μm-thick sections were obtained using a Leica RM 2265 rotary microtome and stained with 0.1% toluidine blue (TBO) for 15 s, rinsed in water, and dried. For transmission electron microscopy, ultrathin sections (70 nm) were obtained using a Leica EM UC6 rotary microtome, subsequently stained with uranyl acetate and lead citrate, and imaged using a Hitachi HT7700 electron microscope.

GUS histochemical assay

The histochemical detection of GUS activity was performed according to a previously described method, with slight modifications (*44*). Briefly, the tissues were fixed in a solution containing 1% MES-KOH (pH 5.6), 0.3% formalin, and 0.3 M mannitol for 30 min at room temperature and washed three times with 50 mM NaH_2PO_4 (pH 7.0). Subsequently, the tissues were infiltrated for 30 min in 50 mM NaH_2PO_4 buffer (pH 7.0) supplemented with 0.5 mM 5-bromo-4-chloro-3-indolyl β-D-glucuronide (X-Gluc), 0.5 mM $K_3Fe(CN)_6$, 0.5 mM $K_4Fe(CN)_6$, and 0.05% Triton X-100 and then incubated at 37°C in the dark for 24 to 48 hours. The tissues were postfixed in 5% formalin and soaked in 5% acetic acid for 10 min at each stage. After undergoing a dehydration process in a graded ethanol series to 100%, the tissues were ready for further examination. Images were taken using an Olympus BX60 microscope equipped with a Nikon DS-Ri1 camera.

Evans blue staining

The water transport activity assay using Evans blue dye has been described previously (*5*). Leaves at the same position from the shoot tips of mock-treated 28-day-old plants or drug-treated plants (kinetin) were collected and stained with Evans blue staining buffer [3% (w/v) Evans blue and 50 mM NaH_2PO_4 (pH 7.0)] for 40 min at room temperature. After being rinsed four times with distilled water, leaves were ready for microscopy analysis.

TBO staining

For visualization of moss leaf cells, 21-day-old gametophores were cleared in Hoyer's medium (Bioroyee) overnight, then washed with deionized water for at least three times, and placed in 2 M NaOH for 2 hours. After washing with deionized water for at least three times, tissues were stained with 0.05% TBO for 5 min, washed with deionized water several times, and left in water until ready for mounting.

Low-humidity treatment analysis

For the low-humidity treatment, we followed the saturated sodium chloride solution method described previously (*5*). The saturated sodium chloride solution was placed in a sealed chamber to prepare the conditions of 70% relative humidity at 25°C. Then, the 8-week-old wild type, *pplas2-3* mutant, *pplas1-2 pplas2-3* double mutant, and double-knockout mutant grown on BCDAT plates were transferred into the above sealed chamber under continuous light for 12 hours and subjected to imaging for checking the wilting status of leaves.

EdU incorporation assay and confocal microscopy

The detection of DNA synthesis was performed according to a previous report (*14*). In short, the 21-day gametophores were excised to expose apices and incubated in liquid BCDAT medium containing 10 μM EdU for a duration as indicated and then fixed in 3.7% formaldehyde for 15 min at room temperature. After being washed twice with 3% bovine serum albumin, samples were subjected to permeabilization with 1% Triton X-100 for 20 min. EdU-labeled nuclei were labeled with Alexa Fluor 555 dye from the Click-iT EdU Imaging Kit (Thermo Fisher Scientific, catalog no. C10338). Confocal microscopy images were taken using a Nikon A1 confocal microscope. To detect the Alexa Fluor 555 signal, a 561-nm laser was used for excitation, and emission was collected at 570 to 620 nm.

Drug treatment

For kinetin, β-estradiol, and roscovitine treatment of *Physcomitrium* gametophore, we developed a deGC methodology to synchronize leaf emergence. To minimize variability in gametophore size, 28-day-old gametophores with almost the same number of leaves were chosen for dissection. Leaves were removed from the base sequentially, with only five visible leaves kept on the shoot tips. The detached gametophores were vertically inserted into the solid BCDAT medium supplemented with kinetin, β-estradiol, or roscovitine at the indicated concentrations and cultured for 7 to 14 days before phenotypic analysis (fig. S12).

For kinetin and BAP treatment in *Arabidopsis*, we followed the detached leaf culture system as described previously (*23*). Leaves between P_8 and P_{10} were detached from seedlings, incubated on MS (Murashige ang Skoog) medium supplemented with kinetin or BAP, and grown for 10 days under short-day conditions before analysis.

For induced overexpression analysis, 28-day-old gametophores of *XVE-PpLAS* transgenic lines were soaked in liquid BCDAT medium supplemented with 1 μM β-estradiol and collected after 12 hours of treatment. For phenotypic analysis, the deGC method was used to treat *XVE-PpLAS* transgenic lines. The detached gametophore tips were cultured on BCDAT medium supplemented with 1 μM β-estradiol for 7 to 14 days (*16*). For Dex treatment, protonemal tissues of *pplas1-3 PpLAS2-GR-3×HA* were cultured on solid BCDAT medium supplemented with 10 μM Dex in 0.1% ethanol or 0.1% ethanol only (mock) for 21 days before phenotypic analyses.

Transcriptomic analysis by RNA-seq

PpLAS-overexpressing *XVE-PpLAS* gametophores (28 days old) were treated with or without 1 μM β-estradiol and collected after 12 hours of treatment. Total RNA was extracted using the AxyPrep Multisource Total RNA Miniprep Kit. Three independent biological replicates were performed for each genotype or treatment. RNA-seq libraries were prepared according to the NEB kit and sequenced using an Illumina HiSeq in the 150-nucleotide paired-end mode. The reads were mapped onto the reference genome of *P. patens* from Phytozome (https://phytozome-next.jgi.doe.gov) using STAR. Transcript expression and differentially expressed genes were determined using the edgeR package, with a cutoff value of >2-fold change and Benjamini-Hochberg false discovery rate of <0.01.

Phylogenetic analysis

Protein sequences of LAS orthologs and paralogs in land plants were retrieved from Phytozome v13 for *A. thaliana*, *P. patens*, *Selaginella moellendorffii*, *Marchantia polymorpha*, *Oryza sativa*, *Solanum lycopersicum*, and *Zea mays*. These protein sequences

were aligned using ClustalW under default parameters. A phylogenetic tree was constructed using the maximum-likelihood method with MEGA7. The LAS paralogs *SCL4* (At5G66770) and *SCL28* (At1G63100) were used as the outgroup in the phylogenetic tree in Fig. 1A. Numbers indicate bootstrap values for their respective branch.

Supplementary Materials

This PDF file includes:
Supplementary Text
Figs. S1 to S21
Tables S1, S2 and S4

Other Supplementary Material for this manuscript includes the following:
Tables S3, S5 and S6

REFERENCES AND NOTES

1. T. Greb, O. Clarenz, E. Schäfer, D. Müller, R. Herrero, G. Schmitz, K. Theres, Molecular analysis of the *LATERAL SUPPRESSOR* gene in *Arabidopsis* reveals a conserved control mechanism for axillary meristem formation. *Genes Dev.* **17**, 1175–1187 (2003).
2. K. Schumacher, T. Schmitt, M. Rossberg, G. Schmitz, K. Theres, The *Lateral suppressor* (*Ls*) gene of tomato encodes a new member of the VHIID protein family. *Proc. Natl. Acad. Sci. U.S.A.* **96**, 290–295 (1999).
3. X. Li, Q. Qian, Z. Fu, Y. Wang, G. Xiong, D. Zeng, X. Wang, X. Liu, S. Teng, F. Hiroshi, M. Yuan, D. Luo, B. Han, J. Li, Control of tillering in rice. *Nature* **422**, 618–621 (2003).
4. S. Cheng, W. Xian, Y. Fu, B. Marin, J. Keller, T. Wu, W. Sun, X. Li, Y. Xu, Y. Zhang, S. Wittek, T. Reder, G. Günther, A. Gontcharov, S. Wang, L. Li, X. Liu, J. Wang, M. Melkonian, Genomes of subaerial zygnematophyceae provide insights into land plant evolution. *Cell* **179**, 1057–1067.e14 (2019).
5. B. Xu, M. Ohtani, M. Yamaguchi, K. Toyooka, M. Wakazaki, M. Sato, M. Kubo, Y. Nakano, R. Sano, Y. Hiwatashi, T. Murata, T. Kurata, A. Yoneda, K. Kato, M. Hasebe, T. Demura, Contribution of NAC transcription factors to plant adaptation to land. *Science* **343**, 1505–1508 (2014).
6. W. Lin, Y. Wang, Y. Coudert, D. Kierzkowski, Leaf morphogenesis: Insights from the moss *Physcomitrium patens*. *Front. Plant Sci.* **12**, 736212 (2021).
7. K. Sakakibara, T. Nishiyama, N. Sumikawa, R. Kofuji, T. Murata, M. Hasebe, Involvement of auxin and a homeodomain-leucine zipper I gene in rhizoid development of the moss *Physcomitrella patens*. *Development* **130**, 4835–4846 (2003).
8. R. Ligrone, J. G. Ducket, K. S. Renzaglia, Conducting tissues and phyletic relationships of bryophytes. *Philos. Trans. R. Soc. Lond. B Biol. Sci.* **355**, 795–813 (2000).
9. H. K. Yip, S. K. Floyd, K. Sakakibara, J. L. Bowman, Class III HD-Zip activity coordinates leaf development in *Physcomitrella patens*. *Dev. Biol.* **419**, 184–197 (2016).
10. K. Landberg, E. R. A. Pederson, T. Viaene, B. Bozorg, J. Friml, H. Jönsson, M. Thelander, E. Sundberg, The moss *Physcomitrella patens* reproductive organ development is highly organized, affected by the two *SHI/STY* genes and by the level of active auxin in the *SHI/STY* expression domain. *Plant Physiol.* **162**, 1406–1419 (2013).
11. D. Cove, The moss, *Physcomitrella patens*. *J. Plant Growth Regul.* **19**, 275–283 (2000).
12. D. G. Schaefer, J. P. Zryd, The moss *Physcomitrella patens*, now and then. *Plant Physiol.* **127**, 1430–1438 (2001).
13. D. Lienard, G. Durambur, M.-C. Kiefer-Meyer, F. Nogué, L. Menu-Bouaouiche, F. Charlot, V. Gomord, J.-P. Lassalles, Water transport by aquaporins in the extant plant *Physcomitrella patens*. *Plant Physiol.* **146**, 1207–1218 (2008).
14. M. Ishikawa, T. Murata, Y. Sato, T. Nishiyama, Y. Hiwatashi, A. Imai, M. Kimura, N. Sugimoto, A. Akita, Y. Oguri, W. E. Friedman, M. Hasebe, M. Kubo, *Physcomitrella* cyclin-dependent kinase a links cell cycle reactivation to other cellular changes during reprogramming of leaf cells. *Plant Cell* **23**, 2924–2938 (2011).
15. Y. Ichihashi, K. Kawade, T. Usami, G. Horiguchi, T. Takahashi, H. Tsukaya, Key proliferative activity in the junction between the leaf blade and leaf petiole of Arabidopsis. *Plant Physiol.* **157**, 1151–1162 (2011).
16. M. Kubo, A. Imai, T. Nishiyama, M. Ishikawa, Y. Sato, T. Kurata, Y. Hiwatashi, R. Reski, M. Hasebe, System for Stable β-estradiol-inducible gene expression in the moss *Physcomitrella patens*. *PLOS ONE* **8**, e77356 (2013).
17. G. E. Schaller, I. H. Street, J. J. Kieber, Cytokinin and the cell cycle. *Curr. Opin. Plant Biol.* **21**, 7–15 (2014).
18. A. Guillory, S. Bonhomme, Phytohormone biosynthesis and signaling pathways of mosses. *Plant Mol. Biol.* **107**, 245–277 (2021).
19. W. B. Yang, S. Cortijo, N. Korsbo, P. Roszak, K. Schiessl, A. Gurzadyan, R. Wightman, H. Jönsson, E. Meyerowitz, Molecular mechanism of cytokinin-activated cell division in *Arabidopsis*. *Science* **371**, 1350–1355 (2021).
20. M. Yamaguchi, H. Kato, S. Yoshida, S. Yamamura, H. Uchimiya, M. Umeda, Control of in vitro organogenesis by cyclin-dependent kinase activities in plants. *Proc. Natl. Acad. Sci. U.S.A.* **100**, 8019–8023 (2003).
21. Y. Wang, Stem cell basis for fractal patterns: Axillary meristem initiation. *Front. Plant Sci.* **12**, 805434 (2021).
22. Q. Wang, A. Hasson, S. Rossmann, K. Theres, Divide et impera: Boundaries shape the plant body and initiate new meristems. *New Phytol.* **209**, 485–498 (2016).
23. Y. Wang, J. Wang, B. Shi, T. Yu, J. Qi, E. M. Meyerowitz, Y. Jiao, The stem cell niche in leaf axils is established by auxin and cytokinin in *Arabidopsis*. *Plant Cell* **26**, 2055–2067 (2014).
24. J. L. Morris, M. N. Puttick, J. W. Clark, D. Edwards, P. Kenrick, S. Pressel, C. H. Wellman, Z. Yang, H. Schneider, P. C. J. Donoghue, The timescale of early land plant evolution. *Proc. Natl. Acad. Sci. U.S.A.* **115**, E2274–E2283 (2018).
25. K. Sakakibara, S. Ando, H. K. Yip, Y. Tamada, Y. Hiwatashi, T. Murata, H. Deguchi, M. Hasebe, J. L. Bowman, KNOX2 genes regulate the haploid-to-diploid morphological transition in land plants. *Science* **339**, 1067–1070 (2013).
26. M. Kubo, M. Udagawa, N. Nishikubo, G. Horiguchi, M. Yamaguchi, J. Ito, T. Mimura, H. Fukuda, T. Demura, Transcription switches for protoxylem and metaxylem vessel formation. *Genes Dev.* **19**, 1855–1860 (2005).
27. I. M. Sussex, N. M. Kerk, The evolution of plant architecture. *Curr. Opin. Plant Biol.* **4**, 33–37 (2001).
28. H. Cui, D. Kong, X. Liu, Y. Hao, SCARECROW, SCR-LIKE 23 and SHORT-ROOT control bundle sheath cell fate and function in *Arabidopsis thaliana*. *Plant J.* **78**, 319–327 (2014).
29. T. T. Tan, H. Endo, R. Sano, T. Kurata, M. Yamaguchi, M. Ohtani, T. Demura, Transcription factors VND1-VND3 contribute to cotyledon xylem vessel formation. *Plant Physiol.* **176**, 773–789 (2018).
30. P. B. Talbert, H. T. Adler, D. W. Parks, L. Comai, The REVOLUTA gene is necessary for apical meristem development and for limiting cell divisions in the leaves and stems of Arabidopsis thaliana. *Development* **121**, 2723–2735 (1995).
31. S. Miyashima, S. Koi, T. Hashimoto, K. Nakajima, Non-cell-autonomous microRNA165 acts in a dose-dependent manner to regulate multiple differentiation status in the Arabidopsis root. *Development* **138**, 2303–2313 (2011).
32. Y. Coudert, O. Novák, C. J. Harrison, A KNOX-cytokinin regulatory module predates the origin of indeterminate vascular plants. *Curr. Biol.* **29**, 2743–2750.e5 (2019).
33. O. Yanai, E. Shani, K. Dolezal, P. Tarkowski, R. Sablowski, G. Sandberg, A. Samach, N. Ori, *Arabidopsis* KNOXI proteins activate cytokinin biosynthesis. *Curr. Biol.* **15**, 1566–1571 (2005).
34. S. Jasinski, P. Piazza, J. Craft, A. Hay, L. Woolley, I. Rieu, A. Phillips, P. Hedden, M. Tsiantis, KNOX action in Arabidopsis is mediated by coordinate regulation of cytokinin and gibberellin activities. *Curr. Biol.* **15**, 1560–1565 (2005).
35. C. Goldy, J. A. Pedroza-Garcia, N. Breakfield, T. Cools, R. Vena, P. N. Benfey, L. de Veylder, J. Palatnik, R. E. Rodriguez, The *Arabidopsis* GRAS-type SCL28 transcription factor controls the mitotic cell cycle and division plane orientation. *Proc. Natl. Acad. Sci. U.S.A.* **118**, e2005256118 (2021).
36. Y. Nomoto, H. Takatsuka, K. Yamada, T. Suzuki, T. Suzuki, Y. Huang, D. Latrasse, J. An, M. Gombos, C. Breuer, T. Ishida, K. Maeo, M. Imamura, T. Yamashino, K. Sugimoto, Z. Magyar, L. Bögre, C. Raynaud, M. Benhamed, M. Ito, A hierarchical transcriptional network activates specific CDK inhibitors that regulate G2 to control cell size and number in Arabidopsis. *Nat. Commun.* **13**, 1660 (2022).
37. R. Sozzani, H. Cui, M. A. Moreno-Risueno, W. Busch, J. M. van Norman, T. Vernoux, S. M. Brady, W. Dewitte, J. A. H. Murray, P. N. Benfey, Spatiotemporal regulation of cell-cycle genes by SHORTROOT links patterning and growth. *Nature* **466**, 128–132 (2010).
38. K. Nakajima, G. Sena, T. Nawy, P. N. Benfey, Intercellular movement of the putative transcription factor SHR in root patterning. *Nature* **413**, 307–311 (2001).
39. H. C. Cui, M. P. Levesque, T. Vernoux, J. W. Jung, A. J. Paquette, K. L. Gallagher, J. Y. Wang, I. Blilou, B. Scheres, P. N. Benfey, An evolutionarily conserved mechanism delimiting SHR movement defines a single layer of endodermis in plants. *Science* **316**, 421–425 (2007).
40. Y. Li, Z. Deng, Y. Kamisugi, Z. Chen, J. Wang, X. Han, Y. Wei, H. He, W. Terzaghi, D. J. Cove, A. C. Cuming, H. Chen, A minus-end directed kinesin motor directs gravitropism in *Physcomitrella patens*. *Nat. Commun.* **12**, 4470 (2021).
41. D. R. Mallett, M. Chang, X. Cheng, M. Bezanilla, Efficient and modular CRISPR-Cas9 vector system for *Physcomitrella patens*. *Plant Direct* **3**, e00168 (2019).
42. Y.-C. Liu, L. Vidali, Efficient polyethylene glycol (PEG) mediated transformation of the moss *Physcomitrella patens*. *J. Vis. Exp.* **50**, 2560 (2011).

43. S. Koshimizu, R. Kofuji, Y. Sasaki-Sekimoto, M. Kikkawa, M. Shimojima, H. Ohta, S. Shigenobu, Y. Kabeya, Y. Hiwatashi, Y. Tamada, T. Murata, M. Hasebe, *Physcomitrella* MADS-box genes regulate water supply and sperm movement for fertilization. *Nat. Plants* **4**, 36–45 (2018).
44. T. Nishiyama, Y. Hiwatashi, K. Sakakibara, M. Kato, M. Hasebe, Tagged mutagenesis and gene-trap in the moss, *Physcomitrella patens* by shuttle mutagenesis. *DNA Res.* **7**, 9–17 (2000).

Acknowledgments: We would like to thank H. Chen (Tsinghua University) and M. Hasebe (National Institute for Basic Biology) for sharing plasmids. We would like to thank X. Xin for analyzing the resequencing data of gene replacement knockout lines and *PpLAS-GUS* reporter lines. **Funding:** This work was supported by National Natural Science Foundation of China grant 31871245 and 32270345 (to Y.W.), National Natural Science Foundation of China grant 32100177 (to Y. Ge), National Key R&D Program of China grant 2019YFA0903902 (to Y.W.), Fundamental Research Funds for the Central Universities (to Y.W.), Bureau of National Tobacco grant 110202001021 (JY-04; to Y.J. and Y.W.), and National Key R&D Program of China grant 2019YFA0903900 (to Y.J.). **Author contributions:** Conceptualization: Y.W. and Y.J. Methodology: Y.W., Y. Ge, and Y. Gao. Investigation: Y. Gao and Y. Ge. Visualization: Y. Ge and Y. Gao Supervision: Y.W. and Y.J. Writing—original draft: Y.W., Y.J., and Y. Ge. Writing—review and editing: Y.W., Y.J., and Y. Ge. **Competing interests:** The authors declare that they have no competing interests. **Data and materials availability:** All data needed to evaluate the conclusions in the paper are present in the paper and/or the Supplementary Materials.

Submitted 30 June 2022
Accepted 20 October 2022
Published 18 November 2022
10.1126/sciadv.add7275